A void growthbased failure model to describe spallation

A. M. Rajendran, M. A. Dietenberger, and D. J. Grove

Citation: J. Appl. Phys. **65**, 1521 (1989); doi: 10.1063/1.342967
View online: http://dx.doi.org/10.1063/1.342967
View Table of Contents: http://jap.aip.org/resource/1/JAPIAU/v65/i4
Published by the American Institute of Physics.

A void growth-based failure model to describe spallation

A. M. Rajendran, M. A. Dietenberger, and D. J. Grove
Structural Integrity Division, University of Dayton Research Institute, Dayton, Ohio 45469

(Received 20 April 1988; accepted for publication 18 October 1988)

A new dynamic failure model to describe void nucleation, growth, and coalescence in ductile metals is reported. The model is based on a pressure-dependent yield criterion for compressible plastic flow. This three-dimensional, plasticity-based continuum damage model is incorporated into a finite difference, wave propagation code. A procedure to determine the failure model parameters is proposed. In this procedure, the model parameters are calibrated based on the ability to match the experimental free-surface velocity history with code simulations. Model parameters for oxygen-free high-conductivity copper have been determined successfully using this procedure.

I. INTRODUCTION

Dynamic failure processes in metals have been studied extensively for the last few decades. There are numerous journal articles, technical reports, and conference proceedings on this subject. Investigators with widely varying backgrounds, such as applied mechanics, metallurgists, and shock physicists, have been contributing to the understanding of dynamic failure. The fundamental failure mechanism associated with dynamic fracture in ductile metals is one which considers the failure process as being initiated by the nucleation of voids around inclusions and their subsequent growth and coalescence as suggested by McClintock.[1] During the last two decades, different approaches have been taken by several investigators[2–11] to apply this mechanism as a means of predicting ductile failure.

The present paper describes a failure model which is based on microvoids nucleation and growth. The effect of damage (void volume fraction) on strength (flow stresses) is incorporated through associated flow rule based plasticity equations. An improved yield function is proposed to describe the effect of pressure and void volume fraction on the von Mises (effective) yield stress. The strain rate effect on the failure process is modeled through a viscoplastic matrix description. Model parameters are determined from a few split Hopkinson bar tensile tests data and a free-surface velocity history of a target plate in a plate impact test. Using the proposed model, spallation in oxygen-free high-conductivity copper (OFHC) is successfully modeled.

II. CONSTITUTIVE/FAILURE MODEL

We identify four phases in the constitutive modeling of damaged materials that were initially intact. The first phase of the modeling is the description of the intact material behavior. Prior to the development of damage, the aggregate is the fully dense matrix material which is usually modeled by incompressible plastic flow theories. The second phase is the description of the damaged material. We require a model to describe the behavior of the aggregate material which contains microvoids/microcracks. In the third phase, depending on the nucleation mechanism, a mathematical description of the process will be required. This phase will also require a model to describe the growth of damage. The last phase of modeling is the coalescence of damage leading to total failure. In the present approach, separate modeling of the coalescence process is not needed. The void growth law is such that the growth rate is rapidly increased as the damage approaches its critical value.

A. Matrix material

The fully dense, void-free matrix material can be modeled through the state variable based viscoplastic constitutive equations of Bodner and Partom (BP model).[12] The BP model in terms of equivalent plastic strain rate $\dot{D}^p_m$ and effective stress Y_m is given by

$$\dot{D}^p_m = \frac{2}{\sqrt{3}} D_0 \exp\left[-\left(\frac{n+1}{2n}\right)\left(\frac{Z}{Y_m}\right)^{2n}\right], \tag{1}$$

where

$$\dot{D}^p_m = \sqrt{\tfrac{2}{3}\dot{\epsilon}^p_{ij}\dot{\epsilon}^p_{ij}}. \tag{2}$$

Z is a state variable. D_0 is the limiting value of the plastic strain rate. The value of D_0 is usually set to 10^8/s for metals. n is a parameter that is mainly related to strain rate sensitivity. The state variable Z describes the overall resistance of the material to plastic flow and it depends on the loading history. The evolution equation for Z is

$$\dot{Z} = m(Z_1 - Z)\dot{W}_p, \tag{3}$$

where $\dot{W}_p$ is the plastic work rate. Z_1 is the maximum value that Z can attain and m is a parameter that embodies the strain-hardening behavior of the material. For highly strain hardening materials like copper, m is described by

$$m = m_0 + m_1 e^{-\alpha W_p}, \tag{4}$$

where m_1 and α are additional model parameters. For less strain-hardening materials, m_1 and α are assumed to be zero. Rajendran, Bless, and Dawicke[13] described the BP model parameter evaluation scheme for three different metals. In their scheme, all the parameters were determined from a few (at least three) tensile split Hopkinson bar stress-strain curves at different strain rates and the steady-state value of the Hugoniot elastic limit (HEL), σ_{HEL}.

Until voids nucleate, the aggregate behavior can be described by the BP model. The plastic flow in the void-free aggregate is incompressible, i.e., the sum of the principal or orthogonal plastic strains is equal to zero. However, the nucleation of voids will introduce dilatation and the plastic

 0021-8979/89/041521-07$02.40

yield behavior will depend not only on the second invariant J_2, but also on the mean stress or pressure. The constitutive model for the aggregate must include these effects. For this purpose, we selected a yield-criterion-based plastic flow rule in which the pressure dependence enters explicitly into the calculations.

B. Modeling of aggregate with voids

We considered a yield-criterion-based approach in the constitutive model formulation. For randomly distributed voids or microcracks contained in the aggregate, the yield behavior will be influenced by not only the second invariant of the deviatoric stress (J_2) but also by the pressure or mean stress (I_1). The following form of the yield function has been considered:

$$A(\rho)J_2 + B(\rho)I_1^2 = \delta(\rho)Y_m^2, \tag{5}$$

where A, B, and δ are functions of relative density, ρ. Y_m is the effective stress in the material. (Note: the subscript m means matrix material and not a tensorial index.) Based on a critical total deformation energy, Doraivelu *et al.*[14] derived the following expressions for A and B:

$$A(\rho) = 2 + \rho^2 \tag{6}$$

and

$$B(\rho) = (1 - \rho^2)/3. \tag{7}$$

The expression for $\delta(\rho)$ under dynamic loading regimes was given by Rajendran, Grove, and Bless[15]:

$$\delta(\rho) = e^{-\beta[(1-\rho)/\rho]}. \tag{8}$$

In general, this function is material dependent while functions A and B are independent of the matrix material behavior. Thus, the yield condition for the aggregate can be written as

$$\Phi = (2 + \rho^2)J_2 + [(1 - \rho^2)/3]I_1^2 - \delta(\rho)Y_m^2 = 0. \tag{9}$$

The viscoplastic strain rates in the aggregate can be calculated using the flow rule derived as

$$\dot{\epsilon}_{ij}^p = \dot{\lambda}\frac{\partial\Phi}{\partial\sigma_{ij}}. \tag{10}$$

The proportionality factor $\dot{\lambda}$ can be obtained using the flow rule in conjunction with the following relationship:

$$(1 - f)Y_m\dot{D}_m^p = \sigma_{ij}\dot{\epsilon}_{ij}^p, \tag{11}$$

where f is the void volume fraction and related to relative density ρ through $f = 1 - \rho$. Note that m is a subscript and not a tensorial index. The above expression was derived from the definition that the total plastic work in the aggregate is entirely due to the plastic work done by the matrix. By combining Eqs. (10) and (11), $\dot{\lambda}$ can be expressed by

$$\dot{\lambda} = [(1 - f)Y_m\dot{D}_m^p] \Big/ \left(\frac{\partial\Phi}{\partial\sigma_{ij}}\sigma_{ij}\right). \tag{12}$$

The plastic strain rates in the aggregate can be written as

$$\dot{\epsilon}_{ij}^p = \left[[(1 - f)Y_m\dot{D}_m^p] \Big/ \left(\frac{\partial\Phi}{\partial\sigma_{r1}}\sigma_{r1}\right)\right]\frac{\partial\Phi}{\partial\sigma_{ij}}. \tag{13}$$

In the constitutive model formulation, the total strain rate is decomposed into elastic and plastic strain rates. The elastic strain rates $\dot{\epsilon}_{ij}^e$ are related to the stress through Hooke's law as

$$\dot{\epsilon}_{ij}^e = D_{ik}\dot{\sigma}_{kj}, \tag{14}$$

where D_{ik} is the inverse of elastic modulus matrix, E_{ik}.

Using the consistency condition which holds during the plastic flow, we can obtain an expression for $\dot{Y}_m$ as

$$\dot{Y}_m = \left[-\left(\frac{\partial\Phi}{\partial\sigma_{ij}}\dot{\sigma}_{ij} + \frac{\partial\Phi}{\partial f}\dot{f}\right)\right] \Big/ \frac{\partial\Phi}{\partial Y_m}. \tag{15}$$

An expression for $\dot{\sigma}_{ij}$ can be obtained from Eq. (14) by replacing the elastic strain rate as the difference between total and plastic strain rates,

$$\dot{\sigma}_{ij} = E_{il}(\dot{\epsilon}_{lj} - \dot{\epsilon}_{ij}^p). \tag{16}$$

We now need an evolution equation to calculate $\dot{f}$ at any given instance of the loading history. The void volume fraction rate $\dot{f}$ contains two parts: one due to the growth of existing voids and the other due to the nucleation of new voids.

C. Void nucleation and growth

The most widely used void nucleation model was the one that was initially used by Chu and Needleman[16] in their analysis of localized necking in biaxially stretched sheets. The model was based on a mechanism in which voids are nucleated due to debonding of inclusions from the matrix. The debonding can occur due to either a stress or a strain criterion or both. The corresponding model is given by

$$\dot{f}_n = F_\sigma(\dot{Y}_m + \dot{P}) + F_\epsilon\dot{D}_m^p, \tag{17}$$

where

$$F_\sigma = (f_1/s_1\sqrt{2\pi})e^{-\frac{1}{2}[(Y_m + P - \sigma_N)/s_1]^2}, \tag{18}$$

and

$$F_\epsilon = (f_2/s_2\sqrt{2\pi})e^{-\frac{1}{2}[(D_m^p - e_n)/s_2]^2}. \tag{19}$$

If the nucleation is only due to the matrix debonding from inclusions, then the total void volume nucleated must be consistent with the volume fraction of second-phase particles. Therefore, the values determined for the parameters f_1 and f_2 must meet this requirement. σ_N and e_N are the mean equivalent stress and strain, respectively, around which the nucleation stress and strain are distributed in a Guassian manner. s_1 and s_2 are the standard deviations of the distributions. These two parameters will control the ranges of stress or strain over which most of the voids can be nucleated.

The growth law can be directly related to the dilatation due to growth of voids in the aggregate. By definition, the growth rate is given by

$$\dot{f}_g = (1 - f)\dot{\epsilon}_{ii}^p, \tag{20}$$

where repeated index means summation and $\dot{\epsilon}_{ii}^p$ are plastic strain rates in the three principal directions and $f = 1 - \rho$. By taking derivatives of the yield function with respect to the stress components and by summing up the plastic strain rates (13), the equation for void growth rate (20) can be written as

$$\dot{f}_g = \frac{3\rho^2\dot{D}_m^p(1 - \rho^2)}{\delta(\rho)}\left(\frac{P}{Y_m}\right). \tag{21}$$

The evolution equation for the void volume fraction is then given by the sum of $\dot{f}_g$ and $\dot{f}_n$ as

$$\dot{f} = (1-f)\dot{\epsilon}^p_{ii} + F_\sigma(\dot{Y}_m + \dot{P}) + F_\epsilon \dot{D}^p_m, \tag{22}$$

where F_σ and F_ϵ are given by Eqs. (18) and (19). Six model parameters have to be determined to describe the void nucleation process, when the process is due to both stress and strain criteria.

When the stress state is triaxial with $(P/Y_m) \gg 1$, the nucleation process is stress controlled; whereas under uniaxial stress states, such as in a thin ring or cylinder under plane stress condition, the mechanism is dominated by strain. It is fairly well established that under high strain rate and high-pressure loading conditions, the void nucleation mechanism is dominated by the pressure (mean stress). To model the spall-type failure, void nucleation due to F_ϵ in Eq. (17) is negligible and, in turn, we can set $F_\epsilon = 0$ in the calculations. Effectively, the void volume fraction model will include only three parameters which can be determined from the plate impact tests data.

The rate equations (1), (3), (13), (15), (16), and (22) must be solved numerically to describe the stress-strain response of a void contained aggregate material. In particular, these equations were carefully rearranged to create a well-behaved set of first-order ordinary differential equations. These equations are solvable by a first-order diagonally implicit Runge–Kutta (DIRK) scheme.[17] A first-order DIRK scheme is designed to be stable, second-order accurate, and efficient for stiff differential equations. The corresponding numerical algorithm was appended to the STEALTH finite difference code.[18] For this purpose several special purpose subroutines were developed. Numerical exercises were conducted using these new subroutines. The exercises were based on a plate impact test simulation. (Note: A description of the plate impact test is given in a later section.) Results showed that the subincremental time steps of the DIRK scheme had to be unrealistically small to sustain a stable solution when $\delta(\rho)$ approached zero. Even for reasonably small time steps, a definite finite difference grid sensitivity was noticed due to the widening gap between the STEALTH time step and the DIRK scheme time step as $\delta(\rho)$ approached zero. Further investigation revealed that this grid sensitivity was due to the exponential form of the $\delta(\rho)$ function [see Eq. (8)]. We investigated this aspect of the modeling as discussed in the following section.

D. A new form for δ(ρ)

The conditions on the coefficient of the matrix effective stress in the yield function is $\delta(\rho) = 1$ at $\rho = 1$ and $\delta(\rho) = 0$ at $\rho = \rho_{cr}$. We proceed initially with the form

$$\delta(\rho) = [g(\rho) - g(\rho_{cr})]/[g(1) - g(\rho_{cr})], \tag{23}$$

which satisfies the conditions on the δ function. A new function for $g(\rho)$ is proposed here as

$$g(\rho) = [\kappa - (N/|N|)(1-\rho)]^N. \tag{24}$$

A negative value of N makes Eq. (24) a hyperbolic power function which we find to be numerically more efficient than the exponential form. This fact has been substantiated through the numerical simulations of a plate impact test configuration. In these simulations, the initial slope of $\delta(\rho)$ at $\rho = 1$ influenced greatly the slope of the spall signal. Thus, we introduce the void growth model parameter, β, where $\beta = \delta'(1)$. With β, N, and ρ_{cr} as model constants, the corresponding value of κ can be solved by a simple iterative scheme.

III. PLATE IMPACT SIMULATIONS

In this section, the plate impact experimental technique is briefly described. Detailed discussions on planar plate impact can be found in Refs. 19 and 20. Determination of the failure model parameters is aided through the simulation of plate impact tests. Simulations are carried out using the STEALTH one-dimensional finite difference code. The effect of each model parameter on the spall behavior is evaluated from the simulation results. A methodology to determine the parameters is outlined. The model also has been successfully used to describe spallation in OFHC copper.

A. Physical features

The impact of a 2-mm-thick copper flyer against a 9-mm-thick OFHC copper target is modeled using the STEALTH code. The constitutive and failure models described in Sec. II were used to characterize the high strain rate behavior of copper. Our first objective is to demonstrate the experimentally observed important physical features of the free-surface velocity profile. In Fig. 1, results from two different simulations are shown. In the first simulation, the model parameters were chosen so that the target spalls. A typical spall signal, as is usually observed in an experiment, can be seen in Fig. 1. In the second simulation the spall is suppressed by choosing a zero value for the nucleation parameter, f_1. The complete unloading of the velocity history as indicated by the dotted line clearly demonstrates the absence of spall in the target.

In Fig. 2, the velocity histories obtained from simulations at different impact velocities are shown. The most important physical features in the velocity profiles are the ve-

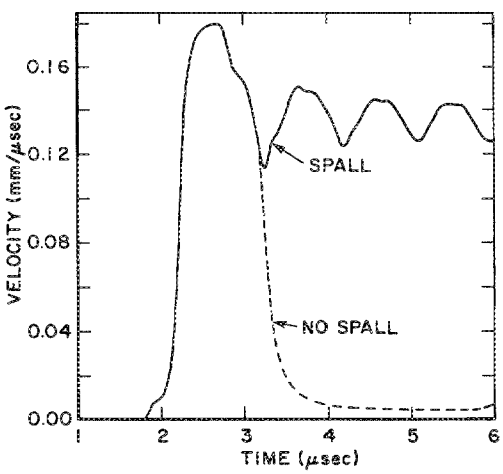

FIG. 1. Simulated velocity history for a target without and with spall failure.

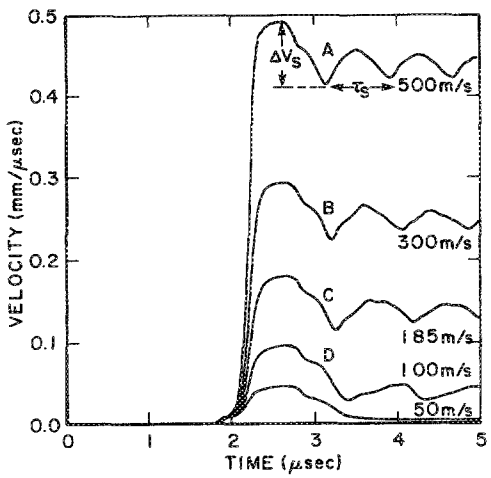

FIG. 2. Simulated free-surface velocity histories at different velocities. (Note: As velocity decreases, at $V = 50$ m/s, no spall occurred.)

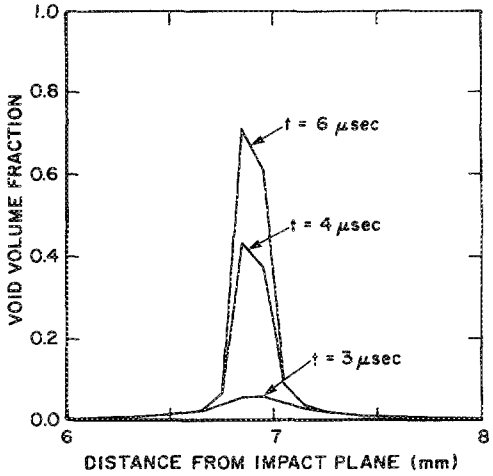

FIG. 4. Model simulated void distribution in the impacted target plate for $t = 3$, 4, and 6 ms.

locity level, ΔV_s, and the time duration or period, τ_s, of the wave transit between the spall plane and the free surface. ΔV_s corresponds to a stress level around which rapid microvoid or microcrack nucleation occurs (note that $\sigma_N = \frac{1}{2}\rho C \Delta V_s$). If the impact velocity is greater than ΔV_s, as in the cases of plots A, B, C, and D in Fig. 2, then spallation will occur, as indicated by the spall signal. However, at an impact velocity of 50 m/s, it can be clearly seen that spall nucleation has not occurred. The tensile stresses in the target at this impact velocity are lower than the mean nucleation threshold stress σ_N (≈ 16 kbar). In the nucleation model, nucleation is assumed to occur at $\sigma_N \pm 3s$, where s is the standard deviation. Figure 3 shows that at velocity $V = 100$ m/s, the tensile peak stress was around 13 kbar, compared to a peak stress of 18 kbar in compression. This is due to void softening of material which reduced the stress levels.

The void volume fraction distribution levels in the target at three different times are shown in Fig. 4. The distribution clearly shows that the maximum void volume fraction is at the spall plane which is around 2 mm (flyer plate thickness) from the free surface (at $x = 7$ mm). The presence of voids at and around the spall plane has been supported by metallographical studies conducted on different materials.[11]

In Fig. 5, the loading path at the spall plane of the target is shown. The void volume levels are shown by dotted lines. Initially the strength is independent of pressure, as can be seen between points A and B. Damage nucleation has not yet initiated and therefore f remains zero. At B, the nucleation occurs. As the pressure increases, the void volume also increases between the loading points B and C. Strength rapidly decreases between points C and D. At 1% void (around D), the void containing aggregate can no longer sustain tensile pressure, so the pressure rapidly decreases as the void volume reaches 10%. Failure (coalescence of voids) occurs between points E and F. Both pressure and strength approach zero as the material completely fails.

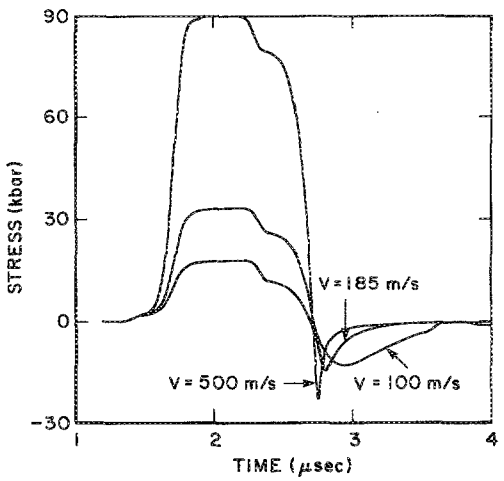

FIG. 3. Simulated stress history at the spall plane. Stress relaxation under tension is shown for three impact velocities: 100, 185, and 500 m/s. (Note: Stress is negative in tension and positive in compression.)

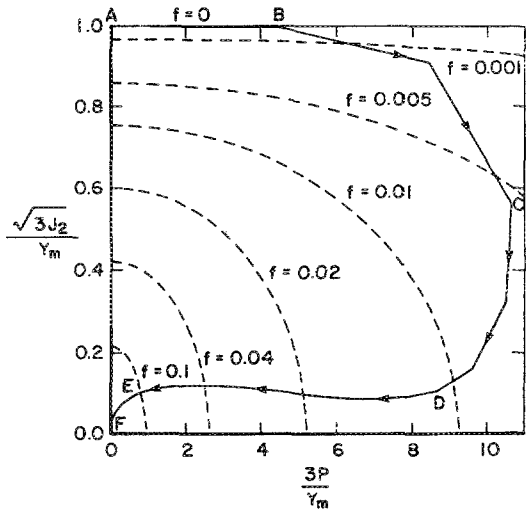

FIG. 5. The loading path ($\sqrt{3J_2}/Y_m$ vs $3P/Y_m$) at the spall plane in a simulation.

B. Stability of the solution

The integration of the ordinary differential equations for the constitutive model by a DIRK scheme is known to be stable and at least second-order accurate. But if the time intervals of the DIRK scheme are much smaller than the time step determined by the Courant criterion in the STEALTH wave propagation code, then the stability and accuracy of the solution becomes uncertain. Depending on the DIRK time step size, the STEALTH stable time step for a particular zone (or element), as determined from the Courant condition, may be reduced by an integer factor ranging from 2 to 10. This factor is initialized to 1, indicating no reduction in the stable time step. Then the factor is either increased by 1 if the last DIRK time step is less than one-tenth of the STEALTH time step, or decreased by 1 if the last DIRK time step is greater than two-tenths of the STEALTH time step. This method allows a gradual, but not necessarily permanent, reduction in the STEALTH stable time step down to one-tenth of the stable time step computed from the Courant condition. Since there is no mathematical criterion of stability for the entire solution, a few numerical exercises were devised to check for solution stability and accuracy. These exercises involved several plate impact simulations. One effective numerical test was to determine if the total momentum and the total energy remained constant during a plate impact simulation. The solution was accepted only if this condition was met. The second exercise was to determine if the entire solution remained essentially the same if the grid size was varied. The results are shown in Fig. 6 for two impact velocities (200 amd 500 m/s) with three different grid sizes. It is possible to absolutely ensure stability and accuracy by forcing the STEALTH time interval to be the same as the DIRK scheme time interval, but this is costly in terms of programming effort and excessive computer time. In any case, numerical exercises to vary the numerical integration and stability parameters should be conducted to optimize the stability, accuracy, and computer time of the solution. The results so far indicate that the solution is stable and reasonably accurate.

C. Sensitivity study

It is important to evaluate the effects of various model parameters ($\sigma_N, f_1, s, \beta, N, f_{cr}$) on the numerically simulated failure process. For this purpose, we conducted a sensitivity study. The sensitivity of the dynamic failure model parameters on the solution (in the free-surface velocity versus time plot) can be checked by varying the values systematically. The variation in the values of the three void nucleation parameters, (σ_N, f_1, and s) were examined first, and then the three void growth parameters (β, N, and f_{cr}) were examined.

An increase in the value of σ_N caused the spall signal to occur later while the solutions during the rebound tend to merge together. Likewise, a decrease in the value of f_1 caused the spall signal to occur later while the solutions during the rebound tend to merge together. It appears the void nucleation parameters σ_N and f_1 have a strong influence on the initial spall signal, but become a negligible influence on the void growth which affects the rebound. The standard deviation s can be defined as a fraction of σ_N. The sensitivity study used three different fractions, 0.125, 0.25, and 0.5. Recall from Eqs. (17) and (18) that the model for void nucleation due to stress follows a Gaussian distribution with mean σ_N, which allows nucleation to occur for a stress range of $\sigma_N \pm 3s$. Since void nucleation in metals can only occur during tension, a practical upper limit for the fraction is one-third. This prevents a negative lower bound for the nucleation stress range. Varying the stress standard deviation, s, had only a minor effect on the spall signal or the rebound.

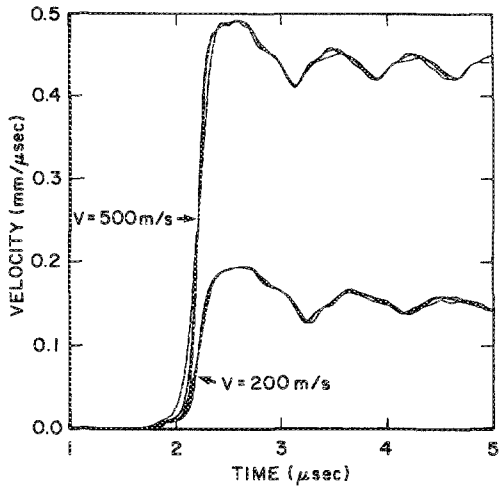

FIG. 6. Demonstration of grid (or mesh) independency of the solution for three different grids at two velocities.

The rebound peak of the spall signal increased for increasing values of the void growth parameters β and $|N|$. The initial slope of the spall signal was less influenced by N than β. Further sensitivity studies showed that the void growth parameter β seems to affect the slope significantly. Taking advantage of the negligible influence of N on the slope, the parameter β can be estimated by matching the spall signal slopes between the simulation and experiment. Varying f_{cr} from 0.6 to 1.0 had a very minimal impact on the spall signal and the rebound. Therefore, we can arbitrarily choose a value of 1 for f_{cr} which is consistent with the definition of f at failure.

In summary, the sensitivity study indicates that the failure model parameters can be systematically determined by matching the simulation results with the spall signal. σ_N can be obtained from the relationship, $\sigma_n = \frac{1}{2}\rho C \Delta V_s$, where ρ is the mass density and C is the wave speed. The value for ΔV_s is available from the velocity history. The value for s can be arbitrarily chosen to be one-fourth of σ_N. A theoretical value of 1 can be assigned for f_{cr}. The only remaining parameters that need to be determined from the spall signal are f_1, β, and N. f_1 can be determined by matching the spall arrival time, β is chosen based on matching the slope of the spall signal, and finally N is selected based on matching the rebound peak of the spall signal. We successfully employed this scheme and determined the model parameters for OFHC copper. The following section describes this effort.

D. Model parameters for OFHC copper

The constitutive and failure models discussed in Sec. II were used to describe OFHC copper at high strain rate loading. Rajendran and Bless[21] determined the BP model parameters from split Hopkinson bar experimental data and the steady-state value of σ_{HEL}. The corresponding parameters are given below:

D_0 (l/s)	m_0 (kbar^{-1})	m_1 (kbar^{-1})	α (kbar^{-1})	n	Z_0 (kbar)	Z_1 (kbar)
10^8	1.1	15.0	150	0.4	8.0	65.5

The plate impact experiment on annealed OFHC copper reported by Rajendran *et al.*[15] was employed in the failure model parameter evaluation. A 2-mm copper flyer was impacted against a 9-mm copper target at an impact velocity of 185 m/s. The free-surface velocity history of the target was determined by velocity interferometer system for any reflector (VISAR) measurements. This velocity history was used in the model parameter calibrations.

Based on the sensitivity study discussed in the preceding section, the failure model parameters are estimated. Out of the six parameters (σ_N, s, f_{cr}, f_1, β, and N), determination of the first three is fairly straightforward. The calculated value for σ_N was 16 kbar, as determined from the measured value of ΔV_s. In order to minimize the number of model parameters by taking advantage of the fact that s and f_{cr} are less sensitive to the failure processes, we arbitrarily assigned $s = 0.25\,\sigma_N$ and $f_{cr} = 1$. We mentioned earlier that the spall signal did not show significant differences for $s = 2$, 4, and 8. Similarly, for $f_{cr} \geqslant 0.5$, the results showed similar trends and therefore a theoretical value of 1 was chosen for f_{cr}.

The remaining parameters β, N, and f_1 were determined by adjusting them until the simulated free-surface velocity matched well with the experimental data. Following the guidelines discussed in the preceding section, f_1 was adjusted to approximately match the spall signal arrival time. Then β was modified until the average initial slope of the spall signal matched with the experimental data. Finally, the value of N was chosen so that the peak velocity of the spall signal rebound matched with the data. The corresponding failure model parameters for OFHC copper are given below:

σ_N (kbar)	s (kbar)	f_1	β	N	f_{cr}
16	4	0.01	65	−2.4	1

It can be seen from Fig. 7 that the simulated free-surface velocity history using the newly developed dynamic failure model in the STEALTH finite difference code compared extremely well with the experimental data. The model parameters were systematically developed using standard high strain rate experimental techniques. The developed model evaluation scheme can be extended to other materials which fail under dynamic loading conditions due to void nucleation, growth, and coalescence.

IV. CONCLUSIONS

Void nucleation and growth-based constitutive and failure models to describe spallation-type failure processes in ductile materials under dynamic loading conditions were presented. The model is three-dimensional and based on micromechanical parameters. Strain rate dependency on the strength (flow stress) and the pressure effect on the plastic flow were also included in the model formulation. New subroutines incorporating a sophisticated numerical procedure were successfully developed to describe the failure model in the STEALTH finite difference code. Numerical stability of the stiff differential equations that describe the model was demonstrated through plate impact simulations.

The matrix material description through the Bodner–Partom model introduces the necessary strain rate dependency into the model. The Bodner–Partom model parameters were determined from the split Hopkinson bar stress-strain data at three different strain rates and the steady-state value of the Hugoniot elastic limit from the plate impact experiments. Rajendran *et al.* described the procedure to determine BP model parameters elsewhere in Ref. 13.

The pressure-dependent yield function served as a plastic potential through which the damage growth and degradation of material strength were effectively modeled. The void nucleation and growth models contained six parameters. The plate impact test simulation results demonstrated that only three parameters, f_1, β, and N, have to be determined by adjusting them to reproduce the experimentally observed free-surface velocity history of the target. Determination of the other three parameters (σ_N, s, f_{cr}) was

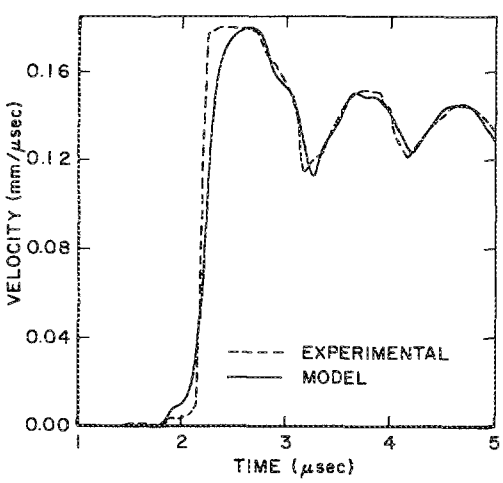

FIG. 7. Comparison between model simulation and the experimental data of the free-surface velocity history.

straightforward and did not require any calibration. However, in the future, the effects of matrix material model parameters on the determination of these three parameters have to be studied additionally.

This model can be implemented into any one-, two-, and three-dimensional finite difference/element wave propagation/dynamic codes. We successfully implemented it into the STEALTH finite difference code and determined the model parameters for OFHC copper. Generality of the proposed three-dimensional failure model in configurations other than plate impact tests is yet to be evaluated. The validity of the model parameters must be evaluated by conducting additional plate impact tests with different thicknesses of both the flyer plate and target.

ACKNOWLEDGMENTS

This work was supported by the U.S. Air Force under Contract No. F33615-86-C-5064. The Project Monitor was Dr. Theodore Nicholas. Partial support was provided by William H. Cook (AFATL/MNW). The authors express their appreciation to W. Cook and Dr. Nicholas for their valuable suggestions and enthusiasms during the model development.

[1]F. A. McClintock, J. Appl. Mech. **35**, 363 (1968).
[2]F. R. Tuler and B. M. Butcher, Int. J. Fracture Mech. **4**, 431 (1968).
[3]S. Cochran and D. Banner, J. Appl. Phys. **48**, 2729 (1977).
[4]D. J. Steinberg and R. W. Sharp, J. Appl. Phys. **57**, 5072 (1981).
[5]D. J. Steinberg, S. G. Cochran, and M. W. Guinan, J. Appl. Phys. **51**, 1498 (1982).
[6]A. M. Rajendran, Doctoral dissertation, University of Washington, Seattle, 1980.
[7]L. Davison, A. L. Stevens, and M. E. Kipp, J. Mech. Phys. Solids **25**, 11 (1977).
[8]J. N. Johnson, J. Appl. Phys. **52**, 2812 (1981).
[9]M. S. Meyers and C. T. Aimone, Prog. Mater. Sci. **28**, 1 (1983).
[10]J. R. Asay and G. I. Kerley, Int. J. Impact Eng. **5**, 69 (1987).
[11]D. R. Curran, D. A. Shockey, and L. Seaman, J. Appl. Phys. **44**, 4025 (1973).
[12]S. R. Bodner and Y. Partom, J. Appl. Mech. **42**, 385 (1975).
[13]A. M. Rajendran, S. J. Bless, and D. S. Dawicke, J. Eng. Mater. Tech. **108**, 75 (1986).
[14]S. M. Doraivelu, H. L. Gegel, J. S. Gunasekara, J. C. Malas, J. T. Morgan, and J. F. Thomas, Int. J. Mech. Sci. **26**, 527 (1984).
[15]A. M. Rajendran, D. J. Grove, and S. J. Bless, in *Shock Waves in Condensed Matter*, edited by S. C. Schmidt and N. C. Holmes (Elsevier, Amsterdam, 1987), p. 359.
[16]C. C. Chu and A. Needleman, J. Eng. Mater. Tech. **102**, 249 (1980).
[17]A. H. Al-Rabeh, Int. J. Comput. Math. **21**, 65 (1987).
[18]R. Hoffman, Electric Power Research Institute Report No. NP-2080, 1981.
[19]C. H. Karnes, in *Mechanical Behavior of Materials Under Dynamic Loads*, edited by U. S. Lindhom (Springer, New York, 1968).
[20]J. R. Asay and J. Lipkin, J. Appl. Phys. **49**, 4242 (1978).
[21]A. M. Rajendran and S. J. Bless, Air Force Wright Aeronautical Laboratory Report No. AFWAL-TR-85-4009, 1985.